Applied Energy 324 (2022) 119678

Contents lists available at ScienceDirect

Applied Energy

journal homepage: www.elsevier.com/locate/apenergy

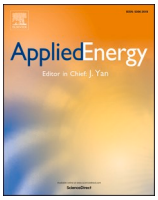

Multi-fault diagnosis for series-connected lithium-ion battery pack with reconstruction-based contribution based on parallel PCA-KPCA

Mina Ma [a], Xiaoyu Li [b], Wei Gao [c], Jinhua Sun [d], Qingsong Wang [d], Chris Mi [c,*]

[a] School of Safety Engineering and Emergency Management, Shijiazhuang Tiedao University, Shijiazhuang 050043, China
[b] Tianjin Key Laboratory of Power Transmission and Safety Technology for New Energy Vehicles, School of Mechanical Engineering, Hebei University of Technology, Tianjin 300401, China
[c] Department of Electrical and Computer Engineering, San Diego State University, 5500 Campanile Drive, San Diego, CA 92182, USA
[d] State Key Laboratory of Fire Science, University of Science and Technology of China, Hefei 230026, China

HIGHLIGHTS

- A multi-fault diagnostic strategy for the series-connected lithium-ion battery pack is proposed.
- The contribution-based PCA is adopted to detect the fault of the battery.
- The reconstruction-based parallel PCA-KPCA is used to estimate the fault waveform.
- Inconsistency, connection fault, and external short circuit are comprehensively diagnosed.
- Algorithm matrix and experiment demonstrate the validity and accuracy.

ARTICLE INFO

Keywords:
Lithium-ion battery safety
Inconsistency
Connection fault
External short circuit
Fault diagnosis

ABSTRACT

Various faults of the lithium-ion battery threaten the safety and performance of the battery system. The early faults are difficult to detect and isolate owing to unobvious abnormality and the nonlinear time-varying characteristics of the battery. Herein, a multi-fault diagnosis strategy is proposed that focuses on detecting and isolating different types of faults, and estimating fault waveforms of the battery, including inconsistency evaluation, virtual connection fault, and external short circuit. First, the principal component analysis (PCA) model of the battery is established and the contribution is employed to detect the abnormity in the battery pack. Once the fault is detected, the parallel kernel principal component analysis (KPCA) technology is adopted to reconstruct the fault waveform of the battery parameters, including ohmic resistance, terminal voltage, and open-circuit voltage. These parameters are jointly taken as fault indexes improving the reliability of fault diagnosis. Finally, the proposed method is verified using amounts of tested data of eight cells in series. The results indicate that the contribution-based PCA method can accurately detect the fault. Furthermore, the reconstruction-based parallel PCA-KPCA can accurately estimate the fault waveform of the faulty battery, which helps investigate the fault degree and causes.

1. Introduction

Electric vehicles (EVs) have become more popular recently due to their capability for sustainable mobility in the future which help combat global climate change, energy crisis, and pollution concerns. Lithium-ion batteries are widely used in EVs owing to the advantages of high energy and power density, long lifespan, low self-discharging, and environmental benefits [1–3]. However, the safety issue of the battery system has restricted the rapid penetration of EVs. Affected by the poor tolerance to abuse, operating conditions, and external environment of the batteries, various faults may occur in the lithium-ion battery system. All kinds of faults may accelerate battery degradation and lead to accidents such as thermal runaway, fire, and explosion [4,5]. Therefore, it is essential to detect and diagnose battery faults for improving the safety and reliability of the battery system [6–8].

In general, the battery faults mainly include overcharge/over-discharge, connection fault, external/internal short circuit, sensor

* Corresponding author.
E-mail address: cmi@sdsu.edu (C. Mi).

https://doi.org/10.1016/j.apenergy.2022.119678
Received 6 January 2022; Received in revised form 4 July 2022; Accepted 10 July 2022

Nomenclature

Acronyms & abbreviations

PCA	principal component analysis
KPCA	kernel principal component analysis
PC	principal component
EVs	electric vehicles
EKF	extended Kalman filters
AEKF	adaptive extended Kalman filter
ISC	internal short circuit
ESC	external short circuit
RLS	recursive least squares
BMS	battery management system
ECM	equivalent circuit model
SOC	state of charge
SOH	state of health
OCV	open-circuit voltage
CPV	cumulative percent variance
PCS	principal component subspace
RS	residual subspace
SPE	squared prediction error
DST	dynamic stress test
DC	direct current
CR	connection resistance
RBF	Radial Basis Function

Notation

U_t	terminal voltage
R_0	ohmic resistance
$\mathbf{X}$	matrix of the U_t, OCV, and R_0 respectively
$\mathbf{R}$	correlation coefficient matrix of the original data $\mathbf{X}$
λ	eigen value
k	the number of principal components
$\mathbf{P}$	loading matrix of $\mathbf{X}$
$\mathbf{T}$	scores matrix of $\mathbf{X}$
$\mathbf{E}$	residual matrix
$\mathbf{t}_i$	scores vector in PCS
$\mathbf{e}_i$	residual vector in RS
SPE_i	residual error between the i-th sample value and the predicted value
$\mathbf{X}_{test,i}$	the i-th sample of real-time monitoring data
$Cont_j^{SPE}$	contribution value of the j-th cell to the statistic SPE
$\mathbf{x}$	actual monitored data
$\mathbf{x}^*$	normal part of the monitored data
$\boldsymbol{\Xi}$	fault space
f	fault amplitude
$\boldsymbol{\kappa}$	kernel matrix
$\widehat{\boldsymbol{\kappa}}$	centered kernel matrix
σ	coefficient of the Gaussian kernel function
$\mathbf{E}'$	the product of $1/m$ and an identity matrix $\mathbf{I}$.
m	the number of samples
n	the number of cells
i	i-th sample
j	j-th cell

fault, inconsistency within the battery pack, and so on. Extensive research for a specific type of fault in the battery system has been carried out. Sidhu et al. [9] proposed a method to detect the occurrence of overcharge and over-discharge by employing a multi-model estimator. Extended Kalman filters (EKF) were applied on normal and fault models to estimate the terminal voltages and generate residuals. Then the proposed algorithm was adopted to evaluate the residual signals. Wu et al. [10] developed a novel fault diagnosis technology based on fuzzy logic to diagnose the overcharge/over-discharge fault. A series of typical abusive tests were conducted to extract fault features. The research connected the fault symptoms with internal fault mechanisms. Yao et al. [11] developed a diagnostic method of connection fault of lithium-ion batteries based on Shannon entropy for EVs. The connection fault was studied by the tests of loose connection bolts of a series-connected battery pack in a vibration environment. The results showed that the ensemble Shannon entropy can accurately predict the time and location of a connection fault. Ma et al. [12] proposed a detection method of virtual connection fault in a series-connected battery pack through an improved Z-score. The cross-voltage test was applied to isolate the connection fault and internal resistance increases of the cell. Besides, the temperature rise rate of the battery was taken as the secondary indicator to improve the robustness of fault detection. For the fault diagnosis of an internal short circuit (ISC), most researchers verify the proposed diagnostic method by paralleling a resistance with the battery, which is still an external short circuit (ESC) in essence. Gao et al. [13] presented a micro-short-circuit diagnostic method for the lithium-ion battery pack in series based on the mean-difference model and EKF. The capacity difference between cells was estimated. The short circuit current and resistance were accurately calculated by employing recursive least squares (RLS). Xia et al. [14] achieved an accurate diagnosis of ESC fault by setting the temperature rise rate, current, and voltage thresholds respectively. It is worth noting that the diagnostic result through the temperature rise rate threshold had a relative delay compared with the changes of current and voltage. Naha et al. [15] developed an effective and robust method for on-board detection of battery short-circuit, in which the current and terminal voltage measured by the battery management system (BMS) were used. A set of features from the recorded data were stored as normal behavior for the initial five charge-discharge cycles. The proposed algorithm can detect the fault 100% with a short-circuit resistance value below 200 Ω. Xiong et al. [16] investigated the characteristics of ESC fault in battery packs through experimental investigation. A two-step equivalent circuit model (ECM) describing the ESC process was established to achieve accurate and fast diagnosis of ESC fault. Liu et al. [17] proposed a diagnostic algorithm for current and voltage sensors fault based on adaptive extended Kalman filter (AEKF). The batteries with maximum and minimum terminal voltage in the series-connected battery pack were modeled to estimate the battery states, respectively. The sensor faults were detected and isolated accurately by evaluating the residuals of the estimated and measured voltage. Qiu et al. [18] put forward a procedure to perform fault diagnosis and inconsistency evaluation based on multi-level Shannon entropy for battery energy storage system.

Owing to the complexity of the battery system and the uncertainty of driving conditions, different types of faults may occur. The diagnosis of a single type fault in a lithium-ion battery pack is highly targeted and not universal. Therefore, it is in urgent demand for a method that can diagnose different types of faults, which is the multi-fault diagnosis method. With the development of research on a single type of fault in the battery pack, some scholars have researched the multi-fault diagnosis of the battery pack, mainly using model-based and data-driven methods.

Liu et al. [19] proposed a multi-fault diagnosis method, including a current sensor, multiple voltage sensors, temperature sensors, and cooling system fault, based on structural analysis. First, a structural model of the battery was built. Then, the multi-residual was generated through the selected structural model of the system. The four types of faults were detected and isolated by setting the fault threshold. Amifia et al. [20] achieved the detection and isolation of the overcurrent/overvoltage fault by presetting the working limit of the current and

voltage. Kang et al. [21] put forward a multi-fault diagnosis method based on an interleaved voltage measurement topology. The topology was explained by constructing a matrix to realize the detection and isolation of the voltage sensor fault, connection fault, ESC, and ISC. The modified correlation coefficient method was used to eliminate the influence of the battery inconsistency and measurement error. This theory needs to add the number of voltage sensors in the battery system. Shang et al. [22] presented an improved sample entropy to realize early diagnosis of the short-circuit fault and open circuit, which solved the difficulty of traditional sample entropy to detect unobvious battery abnormality in the early stages. Park et al. [23] developed a comprehensive diagnosis method for over-discharge and inconsistency among cells based on the maximum available current. Owning to the typical nonlinear time-varying of the battery system, the parameters were identified in real-time and a multi-variate autoregressive model was used to predict the maximum current.

The above studies on multi-fault diagnosis methods are mostly based on model and hardware redundancy. Additionally, the data-driven method is also an effective multi-fault diagnosis method. Gu et al. [24] developed a multi-fault diagnosis system based on the Radial Basis Function (RBF) neural network, which employed the battery current, voltage, temperature, internal resistance, insulation resistance, and state of charge (SOC) as inputs and the fault types as output. The system can accurately diagnose each type of fault and the dangerous degree by training. Khaleghi et al. [25] proposed a real-time battery health diagnosis algorithm based on data-driven using driving cycle profiles. The original voltage was analyzed in time-domain and frequency-domain respectively. The condition indicators extracted in time-domain and frequency-domain were employed to track the state of health (SOH) of the battery online. The proposed method was revealed to have high precision and had the capability of tracking the SOH of the battery with a relative error of less than 1%. Zhang et al. [26] put forward a novel data-driven method for fault diagnosis and thermal runaway warning of the lithium-ion battery pack based on state representation methodology. The proposed method took the normalized voltage as an indicator to extract the real-time state of each cell in the battery pack. The normalized voltage amplified the features of the battery compared with the original voltage so that early faults of the battery can be detected.

In summary, it is still a challenging issue to effectively detect and isolate different types of faults. According to the literature review, there are two knowledge gaps. On one hand, owing to the complexity of the battery system and the uncertainty of driving conditions, different types of faults may occur. The diagnostic methods for one specific type of fault in a lithium-ion battery pack are highly targeted and not universal. It can't comprehensively diagnose different types of faults. On the other hand, the multi-fault diagnosis methods remain lacking, which mainly include model-based and data-driven methods. Model-based methods adopt parameter and state estimation techniques to track changes in the battery. The data-driven method directly extracts useful features from the monitored data onboard to detect faults, regardless of the internal state of the battery. Previous research trends isolate faults by hardware redundancy in existing multi-fault diagnosis methods. Besides, there's currently rarely research attempting to estimate the fault waveform of the battery and considered the inconsistency among cells.

Therefore, to fill these gaps, we propose a multi-fault diagnosis method with reconstruction-based contribution based on principal component analysis (PCA) and kernel principal component analysis (KPCA). To the best of our knowledge, this is the first time that a parallel PCA–KPCA fault detection model is established to diagnose multi-fault of the lithium-ion battery pack. Wang et al. [27] established an estimation model for battery SOC using the KPCA method. The model can extract non-linear factors in parameters. Banguero et al. [28] presented the employ of PCA for the SOH diagnosis of a battery energy storage system. The PCA model is applied to a parameter set associated with the capacity, internal resistance, and open-circuit voltage of a battery energy storage system.

In this work, the proposed method can accurately detect and isolate different types of faults and estimate the fault waveform. Firstly, the recorded terminal voltage in real-time, open-circuit voltage (OCV), and ohmic resistance estimated by the RLS are combined as the fault index parameters. The PCA model of the battery pack is established. The battery pack is evaluated by calculating the contributions of each cell to the PCA statistics. Secondly, the KPCA model of the battery pack is developed to address the nonlinear issue of the battery. The reconstruction-based parallel PCA-KPCA is introduced to estimate the fault waveform of the faulty battery. The estimated fault waveform can provide a scientific basis for the quantitative analysis of the fault causes. Thirdly, the proposed method is verified and analyzed through designed experiments with various types of faults, including the evaluation of inconsistency among cells, virtual connection fault, and ESC. The main contributions of this work are attributed to the following three aspects:

(1) A comprehensive diagnostic strategy for different types of faults in the battery pack is designed, including the inconsistency evaluation among cells, virtual connection fault, and ESC.
(2) The reconstruction-based parallel PCA-KPCA technology can not only locate the faulty battery but also accurately estimate the fault waveform of the battery parameters. The estimated waveform provides a scientific basis for quantitative analysis of fault causes.
(3) Some types of faults will not cause abnormalities in all parameters of the battery. The terminal voltage, OCV, and ohmic resistance are jointly used fault indexes, which improves the reliability of diagnosis in the battery pack. This is non-hardware redundancy.

The remainder of this paper is organized as follows: the diagnostic algorithm is introduced in Section 2. The experimental setup of a battery pack with the inconsistency, virtual connection, and ESC is described in Section 3. The diagnostic results are discussed in Section 4, followed by the key conclusions summarized in Section 5.

2. Methodology

2.1. PCA battery modeling

Principal component analysis (PCA) is a multi-variable statistical technique applied to reduce the dimensionality for a big dataset that tried to lose as little information as possible [29]. PCA applies the historical data of the system under normal operating conditions to establish a statistical model of the variables, which can evaluate the difference among variables and is widely used in the field of fault diagnosis. When a PCA is used, a new variable called principal component (PC) is generated. The first PC contains most of the information of the original data. The second PC indicates a maximum residual variance, and so on. PCA results can be expressed by the scores and loadings matrix. The scores matrix indicates the differences and similarities among variables. The loadings matrix determines the correlation among variables, which helps determine the contributions of each variable [30]. A PCA model of the lithium-ion battery pack in series is established as follows.

A battery pack consists of n cells in series and each cell contains m samples. The original data is organized into a matrix as shown in Eq. (1). $\mathbf{X}$ is the matrix of the U_t, OCV, and R_0 respectively in the battery pack.

$$\mathbf{X} = \begin{bmatrix} x_{11}\ x_{12}\cdots\ x_{1n} \\ x_{21}\ x_{22}\cdots x_{2n} \\ \vdots\ \vdots\ \vdots \\ x_{m1}\ x_{m2}\cdots x_{mn} \end{bmatrix} = (\mathbf{X}_1, \mathbf{X}_2, \cdots, \mathbf{X}_n) \tag{1}$$

where

$$\mathbf{X}_j = \begin{pmatrix} \mathbf{X}_{1j} \\ \mathbf{X}_{2j} \\ \vdots \\ \mathbf{X}_{mj} \end{pmatrix}, (j = 1, 2, \cdots n) \tag{2}$$

First, the original data matrix is normalized by Eq. (3). The data matrix after normalizing is still denoted by **X**.

$$\mathbf{X}_{ij} = \frac{x_{ij} - \overline{x}_j}{s_j}$$

$$\text{where, } \overline{x}_j = \frac{\sum_{i=1}^{m} x_{ij}}{m}, s_j = \sqrt{\frac{\sum_{i=1}^{m} \left(x_{ij} - \overline{x}_j\right)^2}{m-1}} (i = 1, 2, \cdots, m, j = 1, 2, \cdots, n) \tag{3}$$

Then, the correlation coefficient matrix of the original data is calculated, which is the covariance matrix of the normalized data, as shown in Eq. (4):

$$\mathbf{R} = \frac{1}{m-1}\mathbf{X}^{\mathrm{T}}\mathbf{X} \tag{4}$$

Furthermore, the eigenvalues and eigenvectors of the covariance matrix are obtained by calculating as in Eq. (5) to determine the principal component.

$$|\mathbf{R} - \lambda \mathbf{I}_n| = 0 \tag{5}$$

where $\mathbf{I}_n$ is an n-dimensional identity matrix. Vector $\lambda = (\lambda_1, \lambda_2, \ldots, \lambda_n)$ indicates the eigenvalue following $\lambda_1 \geq \lambda_2 \geq \ldots \geq \lambda_n$. Matrix $\mathbf{P}_n = (\mathbf{p}_1, \mathbf{p}_2, \ldots, \mathbf{p}_n)$ is the corresponding eigenvector matrix. The eigenvectors $\mathbf{p}_1, \mathbf{p}_2, \ldots, \mathbf{p}_n$ are the loadings vectors of matrix **X**.

Therefore, the matrix $\mathbf{X} \in \mathbf{R}^{m \times n}$ can be decomposed into the sum of the outer products of n vectors, as shown in Eq. (6).

$$\mathbf{X} = \mathbf{t}_1\mathbf{p}_1^{\mathrm{T}} + \mathbf{t}_2\mathbf{p}_2^{\mathrm{T}} + \cdots + \mathbf{t}_k\mathbf{p}_k^{\mathrm{T}} + \cdots + \mathbf{t}_n\mathbf{p}_n^{\mathrm{T}} = \mathbf{T}\mathbf{P}_k^{\mathrm{T}} + \mathbf{E} \tag{6}$$

where **T** is the scores matrix of the **X** ($\mathbf{t}_k = \mathbf{X}\mathbf{p}_k$), which is essentially the projection of matrix **X** along the direction of the loading vector. The column vector $\mathbf{t}_k$ of the **T** indicates the k-th principal component. k is the number of principal components, which is usually determined according to Cumulative Percent Variance (CPV) [29,31], as shown in Eq. (7). The space where $\mathbf{T}\mathbf{P}_k^{\mathrm{T}}$ is located is named Principal Component Subspace (PCS). The number of PCs k is chosen so that CPV reaches a predetermined value, e.g. 85%. The matrix $\mathbf{E} = \mathbf{t}_{k+1}\mathbf{p}_{k+1}^{\mathrm{T}} + \mathbf{t}_{k+2}\mathbf{p}_{k+2}^{\mathrm{T}} + \cdots + \mathbf{t}_n\mathbf{p}_n^{\mathrm{T}} = \mathbf{X} - \mathbf{T}\mathbf{P}_k^{\mathrm{T}}$ is obtained by predicting X from $\mathbf{T}\mathbf{P}_k^{\mathrm{T}}$. So, **E** represents the residual matrix, which contains the information that is not explained by the principal components. The space where **E** is located is called Residual Subspace (RS).

$$\mathrm{CPV} = \frac{\lambda_1 + \lambda_2 + \cdots \lambda_k}{\lambda_1 + \lambda_2 + \cdots \lambda_n} \times 100\% \tag{7}$$

The above is the process of PCA modeling of the lithium-ion battery pack. The complexity of the original data is reduced by determining the appropriate number of PCs, while the main information of the original variables is retained as much as possible to reduce the dimensionality.

2.2. Fault detection of the contribution-based PCA

The PCA-based fault diagnosis technology is a process of machine learning. The PCA model of the battery pack is established with the normal data. The real-time monitoring data is detected and evaluated using the model. The PCA model projects the observation $\mathbf{X}_i = (x_{i1}, x_{i2}, \ldots, x_{in})$ of the matrix **X** into the PCS to obtain the scores vector $\mathbf{t}_i = (t_{i1}, t_{i2}, \ldots, t_{ik})$ and into the RS to obtain the residual vector $\mathbf{e}_i = (e_{i(k+1)}, e_{i(k+2)}, \ldots, e_{in})$. k indicates the number of PCs. The scores vector and residual vector are summarized into independent statistics: Squared Prediction Error (SPE) and Hotelling T^2 [29,32]. These two statistics respectively represent the extent of the monitored data deviation from the predicted value of the PC model in RS and PCS, which are employed to detect whether an abnormality occurs. In this study, multi-fault detection of the battery pack in series based on the statistic SPE is investigated. The statistic SPE is calculated by Eq. (8).

$$SPE_i = \mathbf{e}_i\mathbf{e}_i^{\mathrm{T}} = \mathbf{X}_{test,i}\left(\mathbf{I} - \mathbf{P}_k\mathbf{P}_k^{\mathrm{T}}\right)\mathbf{X}_{test,i}^{\mathrm{T}} \tag{8}$$

where **I** is the identity matrix. $\mathbf{X}_{test,i}$ represents the i-th sample of real-time monitoring data. SPE_i indicates the residual error between the i-th sample value and the predicted value of PC model. In general, it is detected whether a fault occurs in the system by comparing SPE_i with the SPE control limit [28,33]. However, this method is easily affected by noises and operating conditions. False alarms may occur. Therefore, this paper calculates the contribution of each cell to the SPE, as shown in Eq. (9), to detect faults.

$$Cont_j^{SPE} = sign\left(\mathbf{e}_{test,j}\right) * \mathbf{e}_{test,j}^2, j = 1, 2, \cdots n \tag{9}$$

where $\mathbf{e}_{test} = \mathbf{X}_{test}(\mathbf{I} - \mathbf{P}_k\mathbf{P}_k^{\mathrm{T}}) = \mathbf{X}_{test} - \mathbf{T}_{test}\mathbf{P}_k^{\mathrm{T}}$. $Cont_j^{SPE}$ is the contribution value of the j-th cell to the statistic SPE. If the contribution value is positive, the larger the value, the more it exceeds the normal level. On the contrary, the smaller the value is, the more it is lower than the normal level Therefore, the deviation degree of the battery from the normal level can be utilized to detect battery fault conditions by analyzing the contribution value of each cell to the SPE.

2.3. Fault diagnosis of the reconstruction-based PCA

After an abnormality is detected in the battery pack, the fault waveform is estimated based on the PCA reconstruction to help quantify the fault causes. In this paper, we assume that only one fault occurs in the battery pack at the same time. When a fault occurs, the fault sample vector can be expressed as the following formula:

$$\mathbf{x} = \mathbf{x}^* + \Xi f \tag{10}$$

where **x** is the actual monitored data. **x*** is the normal part of the monitored data. f is the fault amplitude. Ξ indicates the fault space, $\Xi \in \mathbf{I}^{n \times n}$. The column vector $\Xi_j (1 \leq j \leq n)$ of Ξ indicates the fault direction, for example, $\Xi_1 = [0, 0, \ldots, 0]^{\mathrm{T}}$ means fault-free and $\Xi_2 = [0, 1, \ldots, 0]^{\mathrm{T}}$ means fault occurs in cell 2.

The fault reconstruction of data is essential to estimate the normal data corresponding to the fault data to obtain the fault waveform. If cell j fails, the analytical formula for reconstruction is as follows [34]:

$$x_j^* = \frac{\left[\mathbf{c}_{-j}^{\mathrm{T}}\ 0\ \mathbf{c}_{+j}^{\mathrm{T}}\right]\mathbf{x}}{1 - c_{jj}} \tag{11}$$

where $[\mathbf{c}_{-j}^{\mathrm{T}}\ 0\ \mathbf{c}_{+j}^{\mathrm{T}}]$ is the vector after the j-th column of matrix **C** ($\mathbf{C} = \mathbf{P}_k\ \mathbf{P}_k^{\mathrm{T}}$) is replaced by 0. c_{jj} is the j-th row and j-th column of matrix **C**. Therefore, the normal value of the data matrix is estimated and the fault waveform f is calculated to help quantitatively analyze the fault causes.

2.4. KPCA battery modeling

PCA is generally employed to deal with a linear process. For the ternary lithium-ion battery, its ohmic resistance can be approximated as a linear characteristic. However, the terminal voltage and OCV show typical nonlinear. The KPCA has more merits to analyze the nonlinear scenarios. Therefore, after the battery fault is detected through the contribution-based PCA fault detection method, kernel principal component analysis (KPCA) is adopted to reconstruct the terminal voltage and OCV to obtain the fault waveform of the parameters [35].

The key idea of KPCA is to map the data into a higher-dimensional space using a kernel function. A linear relationship is investigated and

PCA is performed in the feature space [36,37]. In general, representative kernel functions include Linear kernel, Polynomial kernel, and Gaussian kernel [38]. In this study, the Gaussian kernel is applied to carry out KPCA and reconstruction on the terminal voltage and OCV data matrix, as shown in Eq. (12).

$$\boldsymbol{\kappa}(x,y)=\exp\left(\frac{-\|\mathbf{x}-\mathbf{y}\|^2}{2\sigma^2}\right),\sigma\in\mathbf{R} \tag{12}$$

where σ is the coefficient of the Gaussian kernel function, also called hyperparameters. Its effect on the Gaussian kernel function is consistent with that of the coefficient in the Gaussian function.

The procedure is as follows:

(1) Normalize the data matrix under normal operating conditions.
(2) Calculate the kernel matrix. The parameters of the Gaussian kernel function are firstly determined and the kernel matrix $\boldsymbol{\kappa}$ is calculated by Eq. (12).
(3) Center the kernel matrix. $\hat{\boldsymbol{\kappa}}=\boldsymbol{\kappa}-\mathbf{E}'\boldsymbol{\kappa}-\boldsymbol{\kappa}\mathbf{E}'+\mathbf{E}'\boldsymbol{\kappa}\mathbf{E}'$, where $\mathbf{E}'$ is equal to the product of $1/m$ and an identity matrix $\mathbf{I}\in\mathbf{R}^{m\times m}$.
(4) The eigenvalues $\lambda=(\lambda_1,\lambda_2,\ldots,\lambda_m)$ $(\lambda_1\geq\lambda_2\geq\ldots\geq\lambda_m)$ of $\hat{\boldsymbol{\kappa}}$ are calculated through eigenvalue decomposition. The corresponding eigenvectors are $\mathbf{P}_m=(\mathbf{p}_1,\mathbf{p}_2,\ldots,\mathbf{p}_m)$.
(5) Calculate the CPV of the eigenvalues according to Eq. (7). The number k of nonlinear PC is determined.
(6) Extract the first k eigenvalues $\lambda_1\geq\lambda_2\geq\ldots\geq\lambda k$ and the corresponding eigenvectors $\mathbf{p}_1,\mathbf{p}_2,\ldots,\mathbf{p}_k$. The eigenvectors are normalized.
(7) Project the kernel matrix $\hat{\boldsymbol{\kappa}}$ to the direction of the eigenvectors to obtain the kernel principal component model of the original data matrix.

2.5. Fault diagnosis of the reconstruction-based KPCA

After the KPCA model is established using the data matrix of terminal voltage and OCV under normal operating conditions, the real-time monitoring data is reconstructed based on the KPCA model to help quantitatively analyze the fault causes.

Similarly, when a fault occurs in the battery pack, the corresponding normal part of the fault data can be expressed as the following formula:

$$\mathbf{x}^*=\mathbf{x}-\boldsymbol{\Xi}f \tag{13}$$

where $\mathbf{x}^*$ is the normal part of the fault data. $\mathbf{x}$ is the actual monitored data. f indicates the fault amplitude. $\boldsymbol{\Xi}$ $(\boldsymbol{\Xi}\in\mathbf{I}^{n\times n})$ is the fault space and the column vector $\Xi_j(1\leq j\leq n)$ of $\boldsymbol{\Xi}$ indicates the direction of the fault.

For the statistic SPE, the estimation formula of the fault waveform is derived as follows [39]:

$$f_i=\frac{\Xi_j\mathbf{B}^{\mathrm{T}}[\mathbf{I}_m+\mathbf{FD}\bar{\mathbf{k}}(\mathbf{x}_i^*)]}{\mathbf{k}^{\mathrm{T}}(\mathbf{x}_i^*)[\mathbf{I}_m+\mathbf{FD}\bar{\mathbf{k}}(\mathbf{x}_i^*)]} \tag{14}$$

where $\mathbf{B}=\begin{bmatrix}\boldsymbol{\kappa}(\mathbf{x}_i^*,\mathbf{x}_1)(\mathbf{x}-\mathbf{x}_1)^{\mathrm{T}}\\ \boldsymbol{\kappa}(\mathbf{x}_i^*,\mathbf{x}_2)(\mathbf{x}-\mathbf{x}_2)^{\mathrm{T}}\\ \vdots\\ \boldsymbol{\kappa}(\mathbf{x}_i^*,\mathbf{x}_m)(\mathbf{x}-\mathbf{x}_m)^{\mathrm{T}}\end{bmatrix}$, $\mathbf{F}=\mathbf{I}_m-\frac{1}{m}\mathbf{I}_m$, $\mathbf{D}=\mathbf{P}_k\boldsymbol{\Lambda}^{-1}\mathbf{P}_k^{\mathrm{T}}$, $\boldsymbol{\Lambda}=$

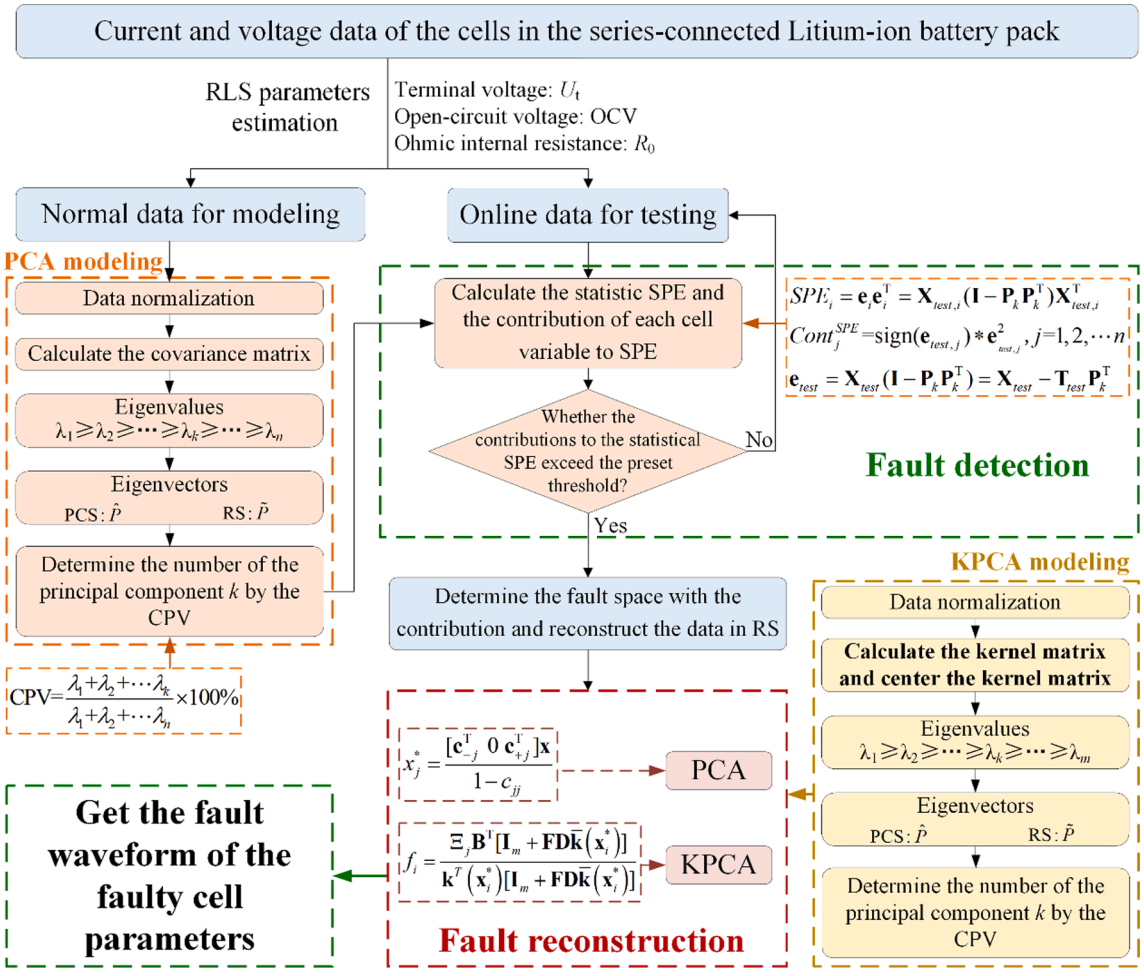

Fig. 1. The schematic process of parallel PCA-KPCA modeling.

diag(λ_1, λ_2, …, λ_k), $\mathbf{k}(\mathbf{x}_i^*)$ is uncentered value of $\boldsymbol{\kappa}(\mathbf{x}_i^*, \mathbf{x}_i)$. $\bar{\mathbf{k}}(\mathbf{x}_i^*)$ is the central value of $\boldsymbol{\kappa}(\mathbf{x}_i^*, \mathbf{x}_i)$.

Therefore, the estimated value f of the fault waveform of the nonlinear parameters matrix is obtained through the above process to help quantitatively analyze the fault causes in combination with the multi-parameter index. The whole process of parallel PCA-KPCA modeling is shown in Fig. 1.

2.6. Multi-fault diagnosis procedure based on parallel PCA-KPCA

This section shows a multi-fault diagnosis procedure for a series-connected battery pack based on parallel PCA-KPCA, as shown in Fig. 2. The multi-fault here refers to different types of faults, including inconsistency assessment among cells, virtual connection fault, and ESC. Firstly, the real-time measured current and terminal voltage of batteries are identified by the RLS online [40]. The ohmic resistance and OCV are obtained. The PCA models of battery parameters are established in the combination of U_t, R_0, and OCV as fault indicators. In this work, the characteristics of the "median cell", which is explained in previous work [41], are adopted as a normal reference to build PCA model. The characteristics of each cell monitored online are for testing. Then, the contributions of each cell parameter to the statistic SPE are calculated, which are compared with the preset threshold. If the contributions do not exceed the preset threshold, the battery pack shows fault-free that can be further evaluated for inconsistency. If the contributions exceed the preset threshold, it is preliminarily detected that a fault has occurred in the battery pack. After a fault is detected, the characteristic parameters, U_t, R_0, and OCV, of the fault cell are reconstructed based on parallel PCA-KPCA. The fault waveforms of the parameters are estimated. In real world applications, the estimated fault waveform helps further quantitively analyze the fault causes of the cell. The battery management system (BMS) control and make decisions based on the diagnostic results to improve the safety of the battery system.

3. Experiment setup

As one of the most critical components in EVs, the battery pack consists of tens to hundreds of cells connected in series and parallel. At each stage of battery manufacturing, screening into groups and use, there will be a certain degree of inconsistency in internal/external parameters such as available capacity, internal resistance, OCV, etc, among the cells in the battery system, which affect the efficiency, safety, and service life of the system. In the operation process of EVs, some factors, such as road condition, environment, and vibration, always affect batteries. Loosening of bolts and welding points in connected cells will inevitably occur, which results in an abnormal increase in connection resistance. Besides, accidental leakage of water into the battery pack, the collision deformation of battery packaging, loose connection plate or wire, etc, may easily trigger the external short circuit. In this study, small-scale fault experiments that consider the inconsistency among cells, virtual connection fault, and external short circuits of the series-connected lithium-ion battery pack are carried out under laboratory conditions to verify the proposed method.

We adopted the LG18650 ternary lithium-ion battery with a rated capacity of 2.5 Ah. The specific parameters are shown in Table 1. The schematic diagram of the experimental setup is shown in Fig. 3. The battery pack structure with eight cells connected in series is presented in Fig. 3(a). The selected batteries are old and have undergone a different using process. The actual capacity of the batteries is given in Table 2. We performed a pre-cycle test on the batteries and fully charged them. The battery pack with eight cells in series is conducted DST [42] cycle at room temperature. The recorded terminal voltage considers the connection resistance of cell-to-cell. In the schematic diagram, the resistors, $R_{1,2}$, $R_{2,3}$, …, $R_{6,7}$, $R_{7,8}$, are used to represent the connection resistance between cells. For example, $R_{1,2}$ is the connection resistance between cell 1 and cell 2 and $R_{5,6}$ is that of cell 5 to cell 6. During the test, we manually loosen the connection wire between cell 3 and cell 4 to simulate a virtual connection fault, while other connections are normally fastened. It is worth noting that the connection resistance caused by the loose fault is unknown, which better reflects the situation in real

Table 1
Specifications of the tested batteries.

Items	Specifications
Nominal capacity	2.5 Ah
Charge ending voltage	4.2 V
Discharge ending voltage	2.75 V
Nominal voltage	3.7 V
Standard charging current	1.25 A
Max charging current	4.0 A
Standard discharging current	0.5 A
Max discharge current	20 A

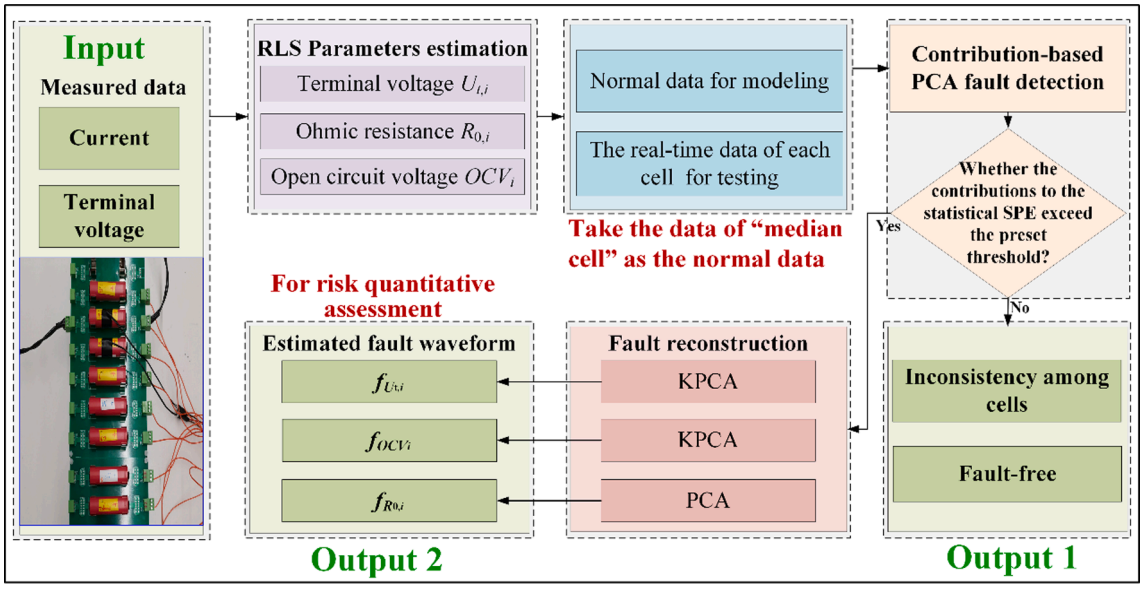

Fig. 2. Multi-fault diagnosis procedure for series-connected battery pack with reconstruction-based contribution based on parallel PCA-KPCA.

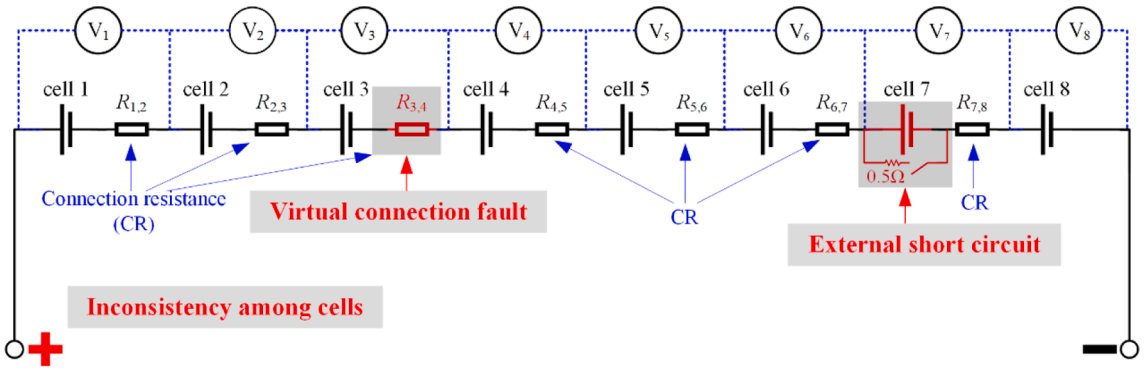

(a) The circuit structure of the battery pack with fault conditions.

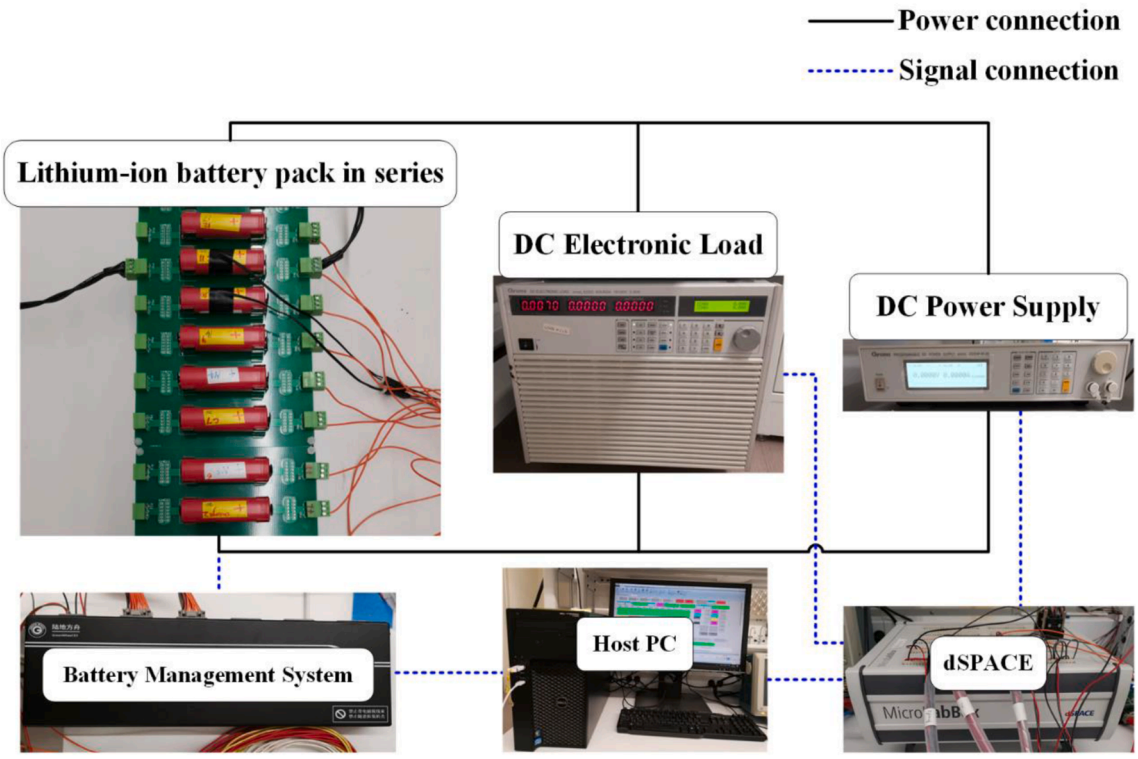

(b) The hardware setup for the battery pack experiment.

Fig. 3. The experimental setup for validation.

Table 2
The actual capacity of the selected batteries.

Cell label	cell 1	cell 2	cell 3	cell 4	cell 5	cell 6	cell 7	cell 8
Actual capacity/Ah	2.2067	2.1219	2.1706	2.1913	2.1448	2.1102	2.1917	2.1472

vehicles. A fixed value resistor with 0.5 Ω is connected in parallel with cell 7. The switch is closed during discharging to simulate an ESC fault in the battery pack. Besides, since the batteries are randomly selected and are all old, there are certain differences among cells, which simulate the inconsistency in the battery pack. The hardware platform for the experiment is provided in Fig. 3(b). A customized BMS is applied to monitor the current and terminal voltage of the battery pack. All the data are collected with dSPACE MicroLabBox and saved by ControlDesk in the host PC. The dis/charge procedures are conducted by the direct current (DC) electronic load and the DC power supply in parallel with the battery pack.

4. Results and discussion

4.1. Experimental results

It is found that the DC electronic load consumes some energy during charging by DC power supply by trial and error. Hence, the charging

process in the DST cycle input file considers the current compensation to implement the standard DST cycle. The DST current distribution is described in Fig. 4. The black solid line is the set current and the red solid line is the recorded actual current through the battery pack. The left picture Fig. 4(a) shows the current during the whole discharging process. One DST cycle for 360 s is enlarged shown in the right picture Fig. 4(b).

The terminal voltage of each cell that takes the faults into account is presented in Fig. 5. It can be observed that the terminal voltage of cell 7 suddenly drops when the short circuit switch closes. Owing to the inconsistency among cells, the fault characteristics of virtual connections are unclear. As can be seen from the enlarged picture on the right, the terminal voltage of cell 3 is higher than that of other cells during charging and lower during discharging. However, the voltage change of cell 3 is not significant compared with other cells. Fault detection is likely to cause misjudgment or missed judgment based on the terminal voltage only. Especially when the battery pack consists of a large number of cells, it is not an effective method to evaluate the fault according to the terminal voltage intuitively. Therefore, the proposed multi-fault diagnosis method is applied to amplify the signal and reconstruct the fault signal. Multi-parameter is considered to improve the reliability of the fault diagnosis.

4.2. Realization of fault detection contribution-based

The OCV and ohmic resistance R_0 of each cell are obtained by online identification based on the RLS, as shown in Fig. 6. Fig. 6(a) depicts the OCV distribution of each cell. The OCV is the same except that of cell 7. The OCV of cell 7 becomes divergent at the end of the discharge. Cell 7 may occur some kinds of fault. The estimated results of R_0 are shown in Fig. 6(b). It can be observed that R_0 of cell 3 is significantly higher than others. Cell 3 may have increased internal resistance or virtual connection fault. A moving window is applied to OCV and R_0 to reduce the influence of noise and improve the robustness of the diagnostic algorithm on the premise of ensuring the authenticity of the data [43], which is equivalent to a low-pass filter. The size of the moving window is set to 200 by trial and error in this paper. Taking cell 1 as an example, Fig. 7 shows the OCV and R_0 results before and after using the moving window. The data through the moving window is smoother without losing the authenticity of the original.

The PCA model is established based on the monitored terminal voltage U_t, the estimated OCV, and R_0 of each cell in the battery pack. Cell 5 is taken as the "median cell" [41] and its characteristics are used as the normal reference to build PCA model. The real-time characteristics of the eight cells are recorded for testing. The contributions of U_t, OCV, and R_0 of each cell to its corresponding statistic SPE are shown in Fig. 8. As can be observed from Fig. 8(a), (b), and (c), the contribution value of each cell characteristic parameter to the corresponding statistic SPE is different from each other. However, there exists no phenomenon that the contribution of one certain cell characteristic parameter to SPE increases or decreases significantly. The contribution difference of each cell characteristic parameter to SPE reflects the inconsistency among cells. If the contribution value of the cell is approximately zero, the corresponding characteristic of the cell is close to the "median cell". If the contribution value of the cell is greater than zero, the corresponding characteristics of the cell are higher than the "median cell" level. Otherwise, the characteristics are smaller than that of the cell. As can be seen from Fig. 8(c), R_0 of cell 2 and cell 6 is greater than that of cell 5. R_0 of cell 1 and cell 4 is lower than that of cell 5. The others are basically the same as that of cell 5.

It can be observed from Fig. 8(d) that the contribution of U_t of cell 3 to the statistic SPE increases or decreases, which corresponds to the process of charging and discharging under DST cycle, respectively. Combined with the analysis of Fig. 8(f), the contribution of R_0 of cell 3 to SPE has increased by orders of magnitude compared to the "median cell". R_0 of cell 3 changes with the process. Therefore, it is verified that U_t and R_0 of cell 3 are abnormal owing to the virtual connection fault instead of the increases in internal resistance. The internal resistance rising of the cell itself is a low-frequency characteristic, which changes with calendar aging or the environment, but does not fluctuate significantly within a discharge cycle. However, the virtual connection fault did not cause the OCV to be abnormal compared to Fig. 8(b) and (e). This is the reason for joint multi-parameter diagnosis. The contribution of U_t of cell 7 to the SPE is significantly reduced at the end of discharging as shown in Fig. 8(g). The contributions of OCV and R_0 are abnormal as presented in Fig. 8(h) and (i). It is judged that an ESC occurred in cell 7 at the end of discharge.

In summary, some types of faults will not cause abnormality of all parameters. For example, a virtual connection fault does not cause abnormal changes in OCV of the cell. Multi-parameter, U_t, OCV, R_0, fault detection can improve the diagnostic reliability by calculating the contributions of each cell according to its corresponding SPE.

4.3. Verification of fault diagnosis reconstruction-based parallel PCA-KPCA

After a fault is detected by the contribution-based PCA, the fault waveform is estimated through reconstruction-based parallel PCA-KPCA to help quantify the fault causes and evaluate the severity. The proposed method is verified and analyzed through the above experimental data in this section. Since the relationship between R_0 and SOC can be approximately regarded as linear, and the U_t and OCV show typical

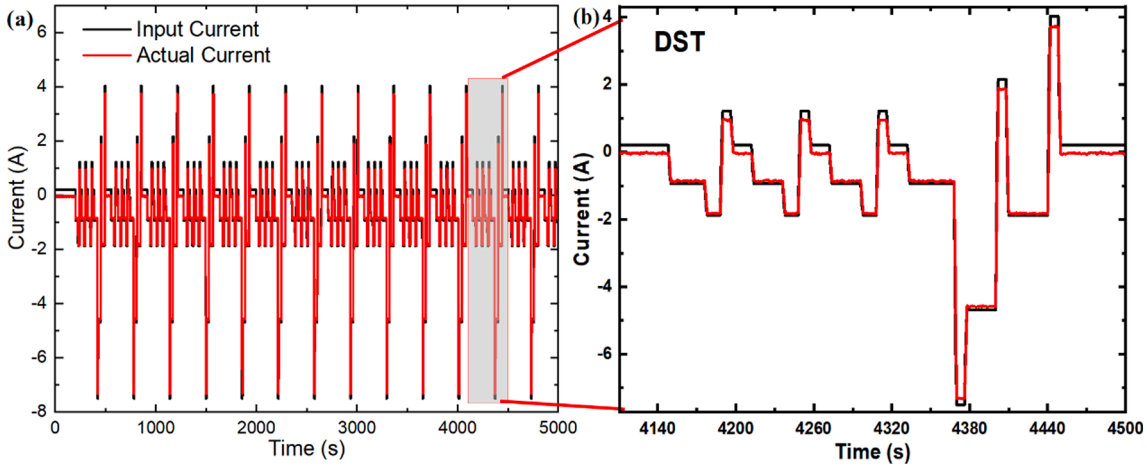

Fig. 4. The current distribution under DST cycle condition. (a) The whole discharge process. (b) the local zoom of (a).

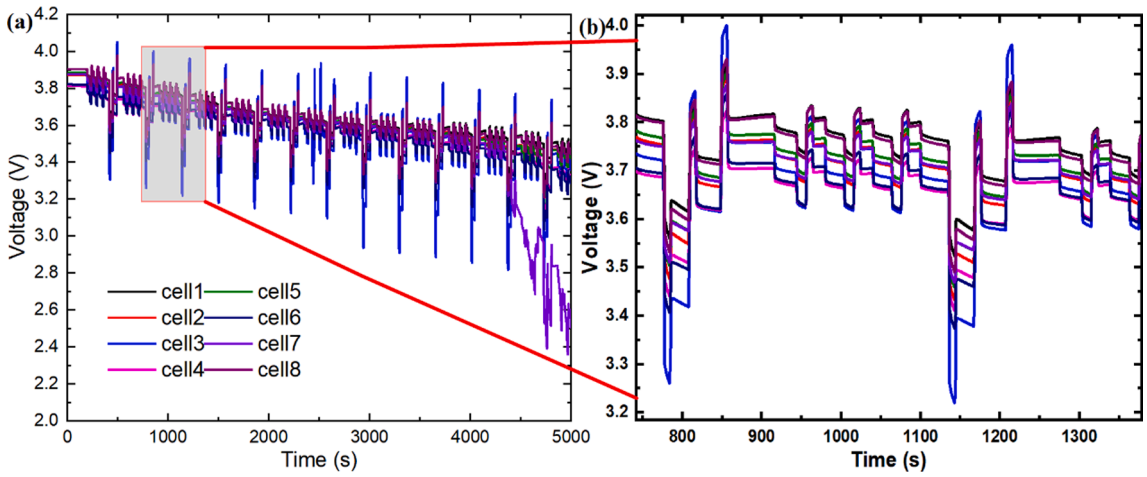

Fig. 5. The terminal voltage distribution of each cell considering faults under DST cycle. (a) The whole discharge process. (b) the local zoom of (a).

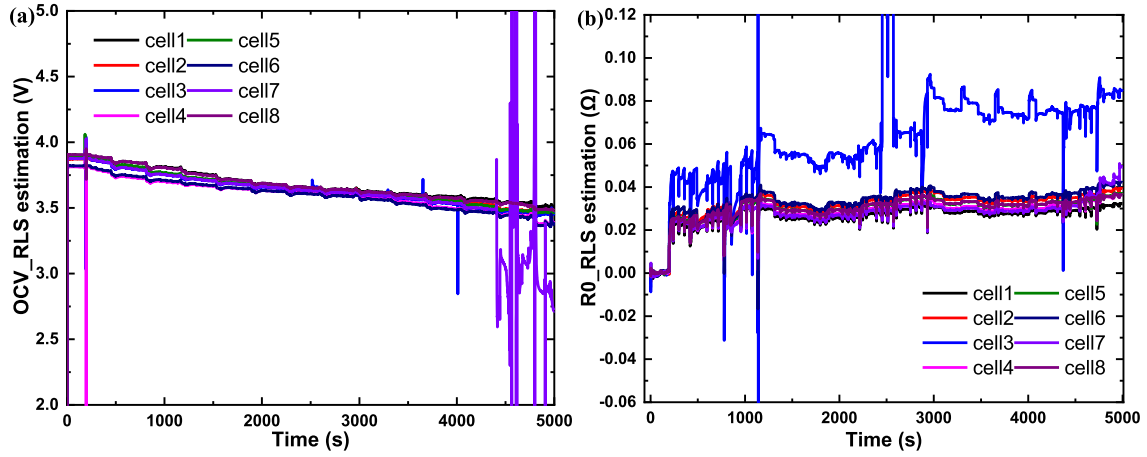

Fig. 6. The estimated results of each cell by the RLS. (a) the estimated OCV of each cell. (b) the estimated ohmic resistance R_0 of each cell.

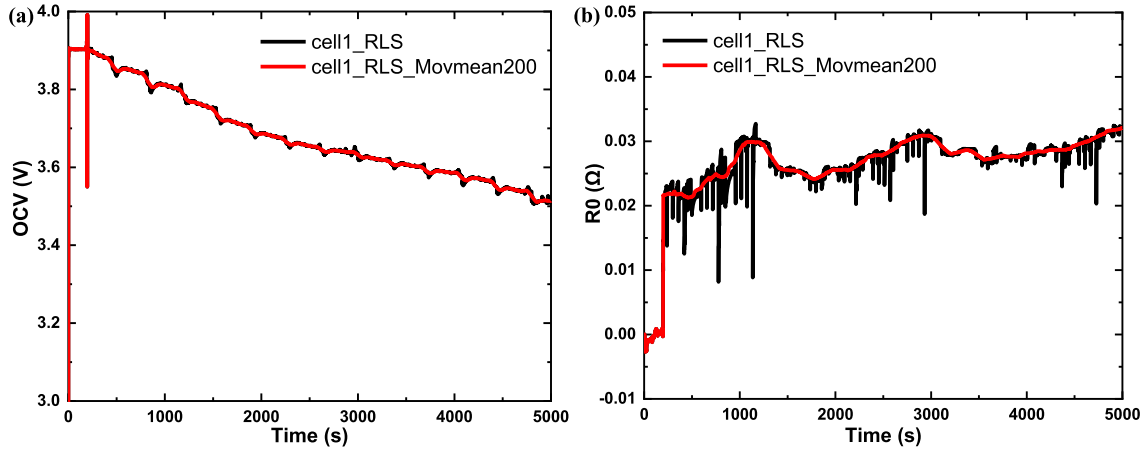

Fig. 7. The parameter results with a moving window. (a) the OCV of cell 1. (b) the R_0 of cell 1.

nonlinear characteristics, parallel PCA-KPCA is adopted to reconstruct the parameters of the faulty cell to estimate the fault waveform. The estimated fault waveform of cell 3 and cell 7 by the method described in Section 2 is shown in Fig. 9. The estimated fault waveform of the parameter is consistent with that of the actual fault waveform. The fault signals of U_t of cell 3 increase when charging and decrease when discharging as presented in Fig. 9(a). In combination with Fig. 9(c), it can be observed that the R_0 of cell 3 increases during the whole DST cycle, especially there is a significant fluction around 2500 s. Cell 3 has occurred a serious virtual connection fault. The battery pack needs to be checked and repaired in time. The fault signals of cell 7 are shown in Fig. 9(d), (e), and (f). U_t drops at about 4300 s. The OCV and R_0 do not

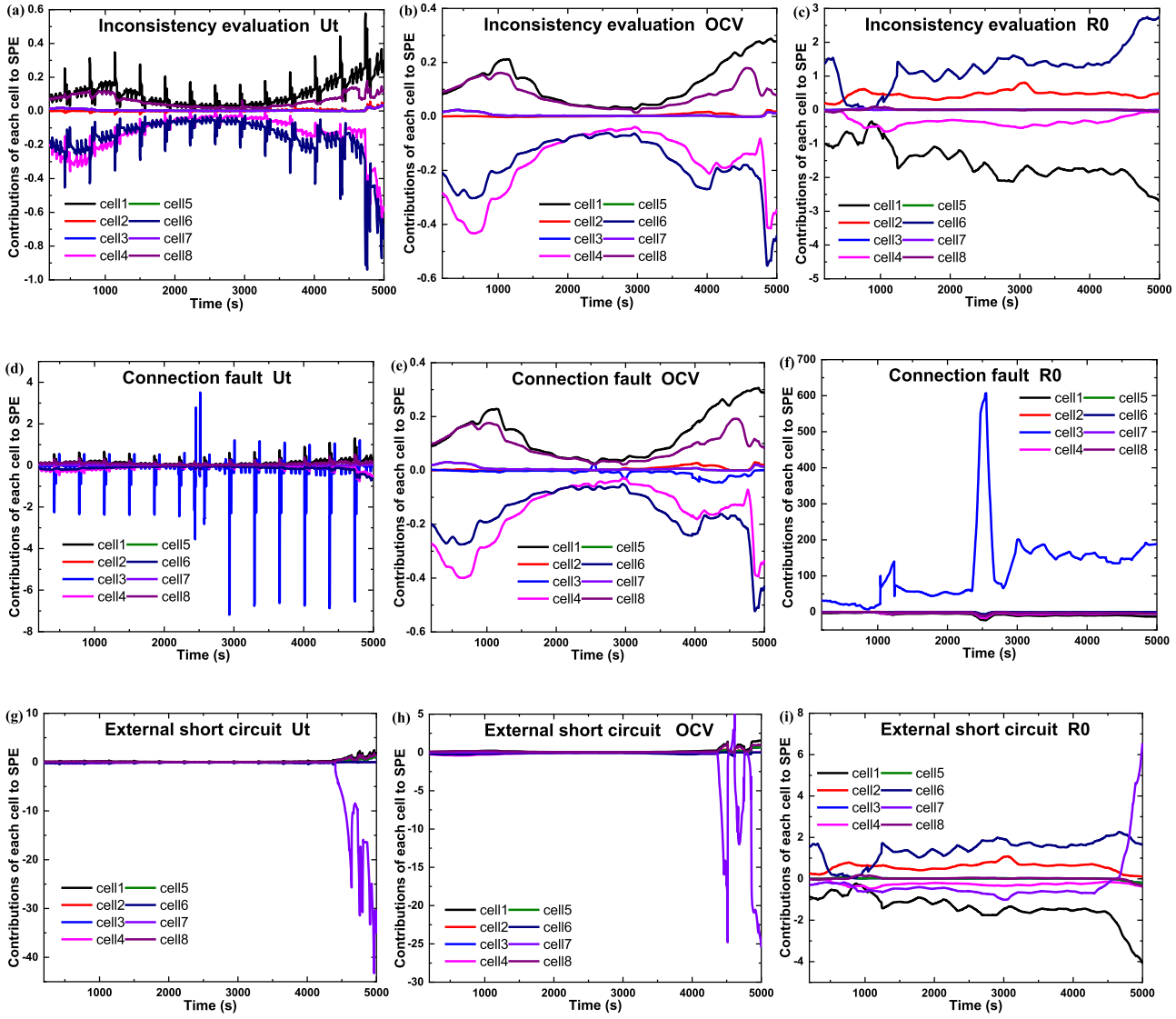

Fig. 8. The contributions of the parameters, U_t, OCV, and R_0, of each cell to its corresponding statistics SPE under different conditions. (a), (b), and (c) are fault-free considering the inconsistency; (d), (e), and (f) are with virtual connection fault; (g), (h), and (i) are with ESC.

converge. It is determined that the positive and negative poles of cell 7 are connected at about 4300 s. If cell 7 continues to work under this condition, cell 7 tends to have a serious over-discharge, which may cause an accident.

Therefore, analysis of experimental results shows that the reconstruction-based parallel PCA-KPCA can accurately estimate the fault signals of U_t, OCV, and R_0 of lithium-ion batteries for analyzing the fault causes, thereby improving the reliability of fault diagnosis.

5. Conclusions

We presented a novel multi-fault diagnosis method for a series-connected lithium-ion battery pack with a reconstruction-based contribution based on parallel PCA-KPCA. The fault detection of contribution-based PCA in the combination of the characteristics of the battery pack is introduced. Thereafter, owing to the typical nonlinear characteristics of lithium-ion batteries, the reconstruction-based parallel PCA-KPCA technology is employed to reconstruct the ohmic resistance, terminal voltage, and open-circuit voltage of the faulty cell. The tested data of eight cells in series are collected to verify the accuracy of the proposed method, including inconsistency among the cells, virtual connection fault, and external short circuit. The results show that the proposed method contribution-based PCA accurately detects the fault in the battery pack and reconstruction-based parallel PCA-KPCA estimate the fault waveform of the faulty battery, which helps to investigate the fault causes. Besides, some types of faults will not cause abnormalities in all parameters of the battery. For example, a virtual connection fault did not cause abnormal changes in open-circuit voltage. Therefore, the terminal voltage, open-circuit voltage, and ohmic resistance are combined to improve the reliability of fault diagnosis based on the model and multivariate statistical analysis methods. Moreover, the reconstruction is performed only when a fault is detected, thereby reducing the computational cost. In practical applications, it needs much more driving data in real scenarios to optimize the diagnostic algorithm to satisfy actual requirements.

Our future research on fault diagnosis of battery systems will focus on the following: on the one hand, employing real-world electric vehicle data to verify and optimize the proposed method to realize the applicability to more types of fault and application of this method in real-world electric vehicles. On the other hand, developing a specific fault signal matrix between features and faults to achieve various fault detection, fault isolation, and fault cause analysis.

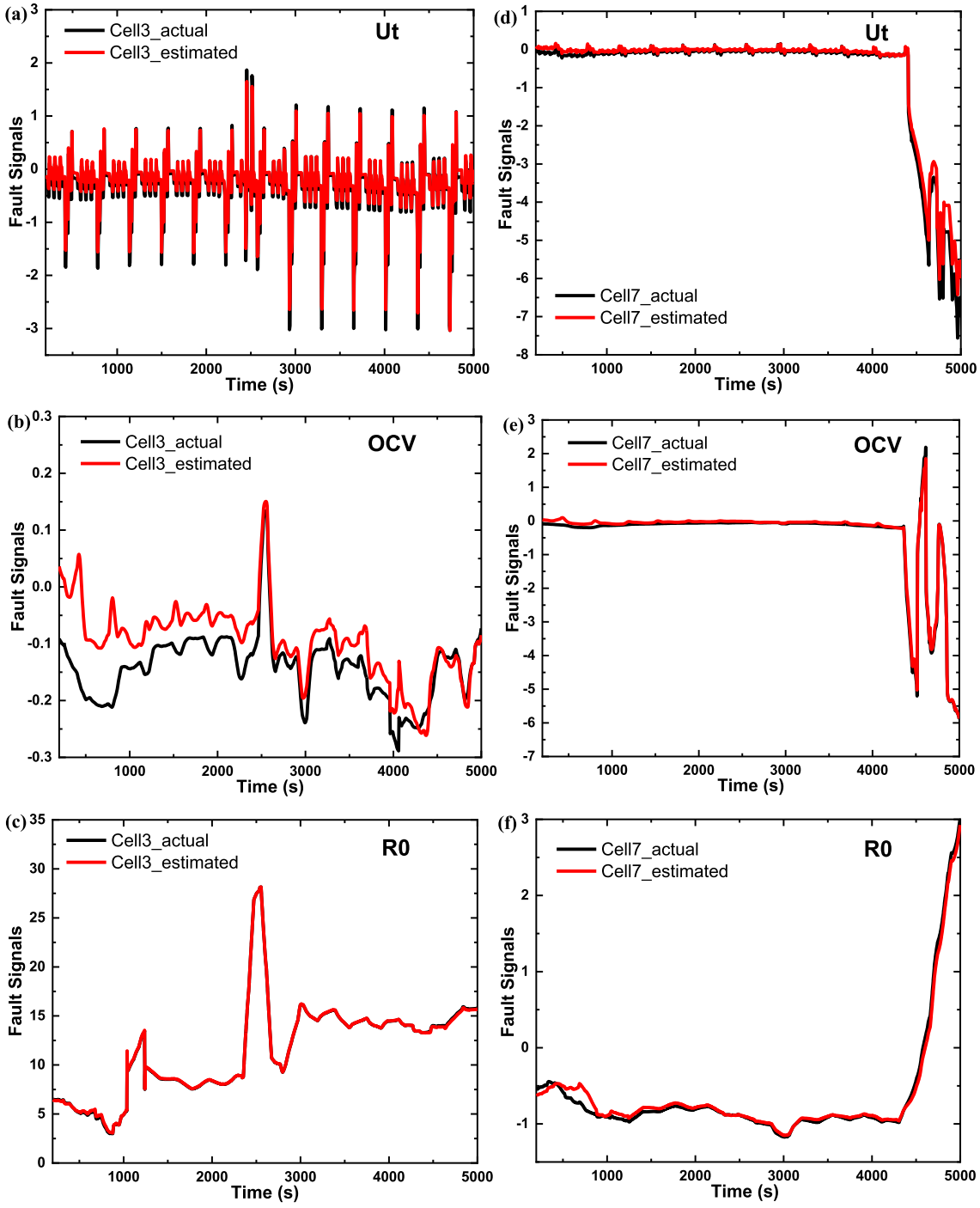

Fig. 9. The estimated fault waveform by reconstruction-based parallel PCA-KPCA. (a), (b), and (c) are the fault waveform of U_t, OCV, and R_0 of cell 3. (d), (e), and (f) are the fault waveform of U_t, OCV, and R_0 of cell 7.

CRediT authorship contribution statement

Mina Ma: Conceptualization, Methodology, Software, Formal analysis, Investigation, Writing – original draft, Visualization. **Xiaoyu Li:** Methodology, Data curation, Writing – review & editing. **Wei Gao:** Software, Validation, Data curation. **Jinhua Sun:** Supervision, Project administration, Funding acquisition. **Qingsong Wang:** Supervision, Project administration, Funding acquisition, Writing – review & editing. **Chris Mi:** Resources, Supervision, Funding acquisition, Writing – review & editing.

Declaration of Competing Interest

The authors declare that they have no known competing financial interests or personal relationships that could have appeared to influence the work reported in this paper.

Data availability

The data that has been used is confidential.

Acknowledgments

This work is supported by the National Natural Science Foundation of China (No. U2033204), the Key Research and Development Plan of Anhui Province (No. 202104a07020003), the University Synergy Innovation Program of Anhui Province (No. GXXT-2020-079). Dr. Q.S. Wang is supported by Youth Innovation Promotion Association CAS (No. Y201768) and Dr. M.N. Ma is supported by the National Construction of High-Level University Public Graduate Project.

References

[1] Etacheri V, Marom R, Elazari R, Salitra G, Aurbach D. Challenges in the development of advanced Li-ion batteries: a review. Energy Environ Sci 2011;4:3243–62.
[2] Varga BO. Electric vehicles, primary energy sources and CO2 emissions: Romanian case study. Energy 2013;49:61–70.
[3] Tarascon J-M, Armand M. Issues and challenges facing rechargeable lithium batteries. Nature 2001;414(6861):359–67.
[4] Balakrishnan PG, Ramesh R, Prem Kumar T. Safety mechanisms in lithium-ion batteries. J Power Sources 2006;155(2):401–14.
[5] Wang Q, Ping P, Zhao X, Chu G, Sun J, Chen C. Thermal runaway caused fire and explosion of lithium ion battery. J Power Sources 2012;208:210–24.
[6] Rezvanizaniani SM, Liu Z, Chen Y, Lee J. Review and recent advances in battery health monitoring and prognostics technologies for electric vehicle (EV) safety and mobility. J Power Sources 2014;256:110–24.
[7] Hu X, Zhang K, Liu K, Lin X, Dey S, Onori S. Advanced fault diagnosis for Lithium-ion battery systems: a review of fault mechanisms, fault features, and diagnosis procedures. IEEE Ind Electron Mag 2020;14:65–91.
[8] Xiong R, Sun W, Yu Q, Sun F. Research progress, challenges and prospects of fault diagnosis on battery system of electric vehicles. Appl Energy 2020;279:115855.
[9] Sidhu A, Izadian A, Anwar S. Adaptive Nonlinear Model-Based Fault Diagnosis of Li-Ion Batteries. IEEE Trans Ind Electron 2015;62:1002–11.
[10] Wu C, Zhu C, Ge Y. A New Fault Diagnosis and Prognosis Technology for High-Power Lithium-Ion Battery. IEEE Trans Plasma Sci 2017;45(7):1533–8.
[11] Yao L, Wang Z, Ma J. Fault detection of the connection of lithium-ion power batteries based on entropy for electric vehicles. J Power Sources 2015;293:548–61.
[12] Ma M, Wang Y, Duan Q, Wu T, Sun J, Wang Q. Fault detection of the connection of lithium-ion power batteries in series for electric vehicles based on statistical analysis. Energy 2018;164:745–56.
[13] Gao W, Zheng Y, Ouyang M, Li J, Lai X, Hu X. Micro-short-circuit diagnosis for series-connected Lithium-ion battery packs using mean-difference model. IEEE Trans Ind Electron 2019;66:2132–42.
[14] Xia B, Chen Z, Mi C, Robert B. External short circuit fault diagnosis for lithium-ion batteries. Transportation Electrification Conference and Expo (ITEC), 2014 IEEE. IEEE; 2014. p. 1–7.
[15] Naha A, Khandelwal A, Hariharan KS, Kaushik A, Yadu A, Kolake SM. On-board short circuit detection of Li-ion batteries undergoing fixed charging profile as in smartphone applications. IEEE Trans Ind Electron 2019;66:8782–91.
[16] Xiong R, Yang R, Chen Z, Shen W, Sun F. Online fault diagnosis of external short circuit for lithium-ion battery pack. IEEE Trans Ind Electron 2020;67:1081–91.
[17] Liu Z, He H. Sensor fault detection and isolation for a lithium-ion battery pack in electric vehicles using adaptive extended Kalman filter. Appl Energy 2017;185:2033–44.
[18] Qiu Y, Cao W, Peng P, Jiang F. A novel entropy-based fault diagnosis and inconsistency evaluation approach for lithium-ion battery energy storage systems. J Energy Storage 2021;41:102852.
[19] Liu Z, He H, Ahmed Q, Rizzoni G. Structural analysis based fault detection and isolation applied for a Lithium-ion battery pack. IFAC-PapersOnLine 2015;48(21):1465–70.
[20] Amifia LK, Widayat SA, Cahyadi AI, Wahyunggoro O. Fault detection design and simulation based on battery modelling. In: AIP Conference Proceedings: AIP Publishing LLC; 2016. p. 090008.
[21] Kang Y, Duan B, Zhou Z, Shang Y, Zhang C. A multi-fault diagnostic method based on an interleaved voltage measurement topology for series connected battery packs. J Power Sources 2019;417:132–44.
[22] Shang Y, Lu G, Kang Y, Zhou Z, Duan B, Zhang C. A multi-fault diagnosis method based on modified Sample Entropy for lithium-ion battery strings. J Power Sources 2020;446:227275.
[23] Park J, Kim J, Lee M, Kwon S, Na W, Kim J. Analysis of the cell-to-cell imbalance in battery pack based on the over-discharge prognosis and maximum available current prediction for comprehensive management strategy. 2021 IEEE Applied Power Electronics Conference and Exposition (APEC); 2021. p. 2714-8.
[24] Gu A, Zhang X. Fault diagnosis system for power battery based on RBF neural network. Chinese J Power Sources 2016;40:1943–5.
[25] Khaleghi S, Firouz Y, Van Mierlo J, Van den Bossche P. Developing a real-time data-driven battery health diagnosis method, using time and frequency domain condition indicators. Appl Energy 2019;255:113813.
[26] Zhang K, Hu X, Liu Y, Lin X, Liu W. Multi-Fault Detection and Isolation for Lithium-Ion Battery Systems. IEEE Trans Power Electron 2022;37(1):971–89.
[27] Wang H, Wang Y, Yao Z, Yu Z. Lithium-ion power batteries soc estimation based on pca. Int J Performability Eng 2018;14:1618.
[28] Banguero E, Correcher A, Pérez-Navarro Á, García E, Aristizabal A. Diagnosis of a battery energy storage system based on principal component analysis. Renew Energy 2020;146:2438–49.
[29] Jackson JE, Mudholkar GS. Control procedures for residuals associated with principal component analysis. Technometrics 1979;21(3):341–9.
[30] Abdi H, Williams LJ. Principal component analysis. J Wiley Interdisciplinary Rev: Comput Statist 2010;2(4):433–59.
[31] Jeng J-C. Adaptive process monitoring using efficient recursive PCA and moving window PCA algorithms. J Taiwan Inst Chem Eng 2010;41(4):475–81.
[32] Li S, Wen J. A model-based fault detection and diagnostic methodology based on PCA method and wavelet transform. Energy Build 2014;68:63–71.
[33] Bo L, Xinsheng W. Fault detection and reconstruction for micro-satellite power subsystem based on PCA. In: 2010 3rd International Symposium on Systems and Control in Aeronautics and Astronautics; 2010. p. 1169–73.
[34] Wang W. The research on the sensor fault detection and diagnosis of the central air-conditioning water system based on PCA: Hunan; 2014.
[35] Jiang QC, Yan XF. Parallel PCA-KPCA for nonlinear process monitoring. Control Eng Pract 2018;80:17–25.
[36] Schölkopf B, Smola A, Müller K-R. Nonlinear component analysis as a kernel eigenvalue problem 1998;10:1299–319.
[37] Lee J-M, Yoo C, Choi SW, Vanrolleghem PA, Lee I-B. Nonlinear process monitoring using kernel principal component analysis. Chem Eng Sci 2004;59(1):223–34.
[38] Soh W, Kim H, Yum B-J. Application of kernel principal component analysis to multi-characteristic parameter design problems. Ann Oper Res 2018;263(1-2):69–91.
[39] Alcala CF, Qin SJ. Reconstruction-based contribution for process monitoring with kernel principal component analysis. Ind Eng Chem Res 2010;49(17):7849–57.
[40] Ma M, Duan Q, Zhao C, Wang Q, Sun J. Faulty Characteristics and Identification of Increased Connecting and Internal Resistance in Parallel-Connected Lithium-ion Battery Pack for Electric Vehicles. IEEE Trans Veh Technol 2020;69:10797–808.
[41] Ma M, Duan Q, Li X, Liu J, Zhao C, Sun J, et al. Fault diagnosis of external soft-short circuit for series connected lithium-ion battery pack based on modified dual extended Kalman filter. J Energy Storage 2021;41:102902.
[42] Consortium USAB. Electric vehicle battery test procedures manual. USABC; Jan. 1996.
[43] Lai X, Yi W, Kong X, Han X, Zhou L, Sun T, et al. Online detection of early stage internal short circuits in series-connected lithium-ion battery packs based on state-of-charge correlation. J Energy Storage 2020;30:101514.